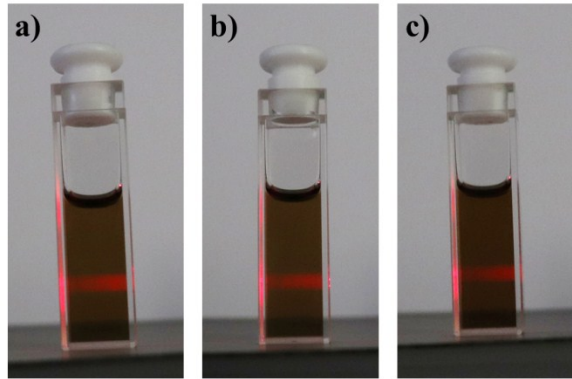


**Supporting Information to**  
**Patching Laser-Reduced Graphene Oxide with Carbon**  
**Nanodots**

Volker Strauss, Mit Muni, Arie Borenstein, Bolortuya Badamdorj, Tobias Heil, Matthew D. Kowal,  
Richard Kaner

<b>Sample overview .....</b>	<b>19</b>
<b>Scanning electron microscopy .....</b>	<b>20</b>
<b>Raman spectroscopy.....</b>	<b>21</b>
<b>Transmission electron microscopy and electron energy loss spectroscopy.....</b>	<b>22</b>
<b>Specific surface area measurements .....</b>	<b>23</b>
<b>Voltammetry .....</b>	<b>23</b>
Three-electrode measurements.....	24
Reference measurements in organic electrolyte .....	25
Capacitance .....	25
Galvanostatic charge-discharge measurements.....	26
Electrochemical impedance spectroscopy.....	27

## Sample overview



**Figure S1.** Photograph of precursor solutions of 1, 3, and 6 in NMP after one week under illumination with a laser pointer demonstrating the Tyndall effect.

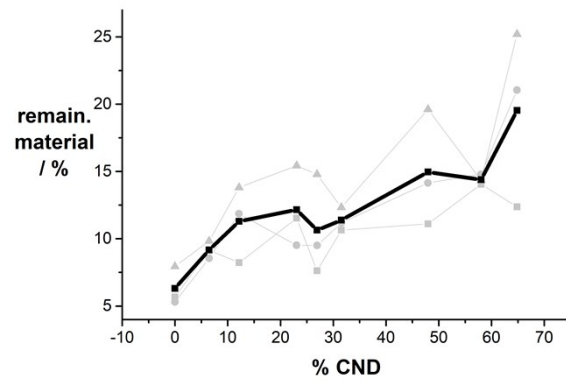


**Figure S2.** Percentage of the remaining mass of the films after laser-reduction obtained from a series of experiments (shown in gray).

## Scanning electron microscopy

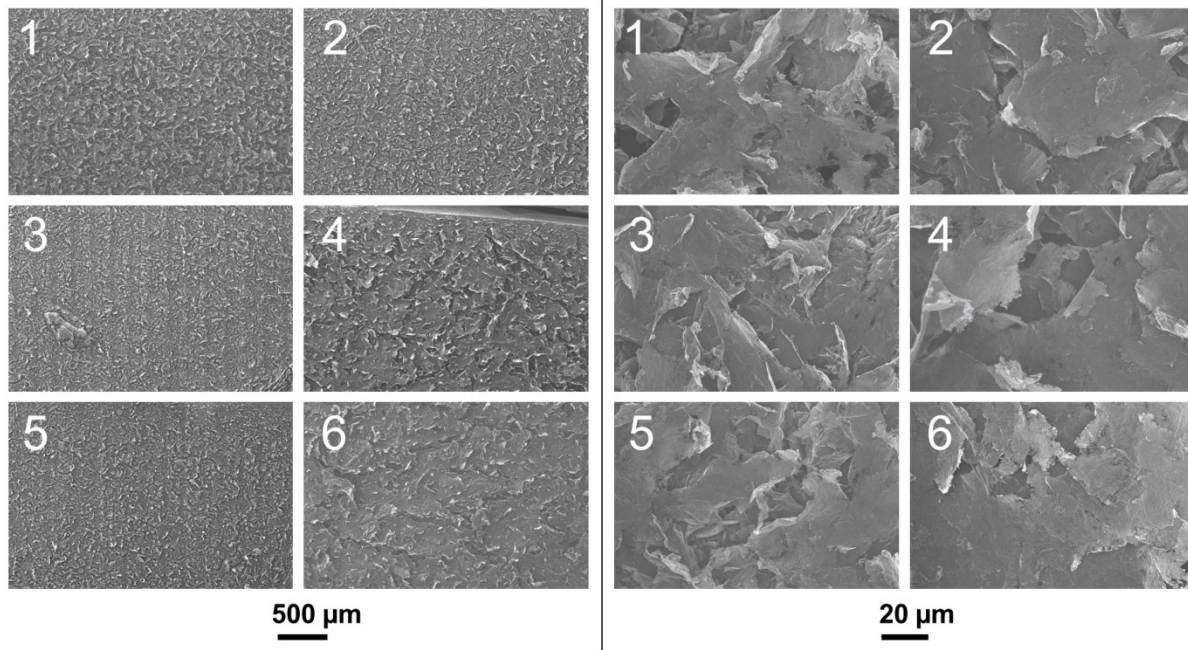


**Figure S3.** SEM images of laser-converted films of samples 1 – 6 from top left down to bottom right at low-magnification (left) and high-magnification (right), see scale bars.

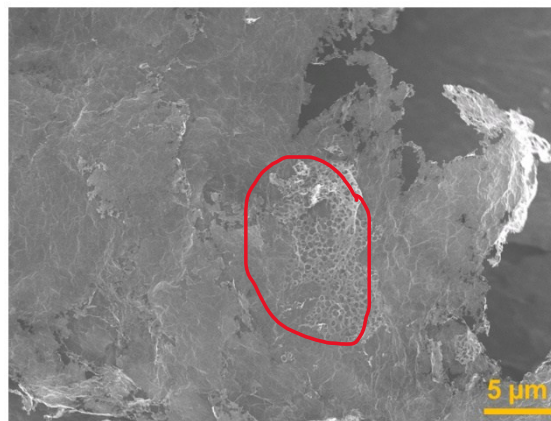


**Figure S4.** SEM image of a laser-converted film of sample 6 showing a converted pattern with excess CNDs.

## Raman spectroscopy

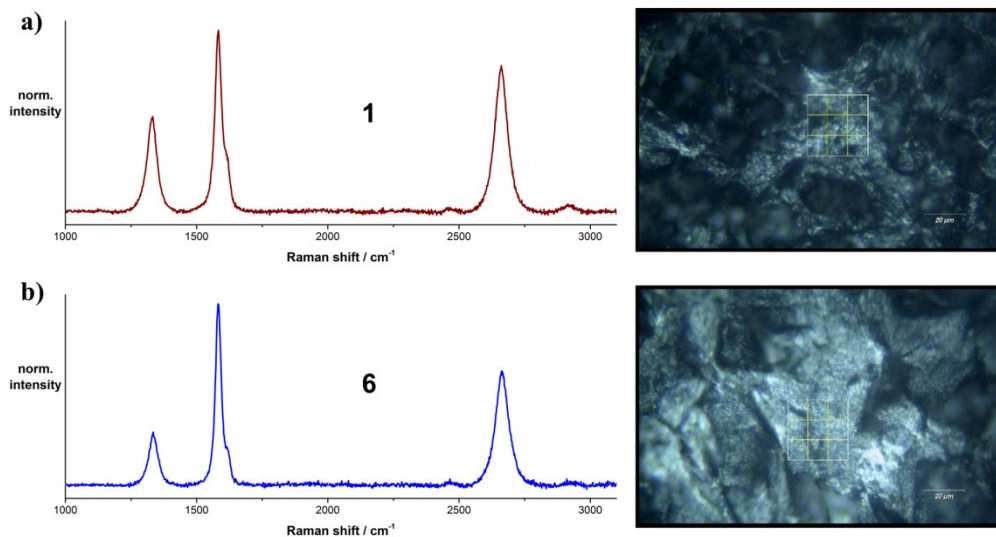


*Figure S5. Averaged Raman spectrum obtained from a map composed of 16 spots (depicted on the right) of laser-reduced samples a) 1 and b) 6 using a 633 nm laser as the excitation source.*

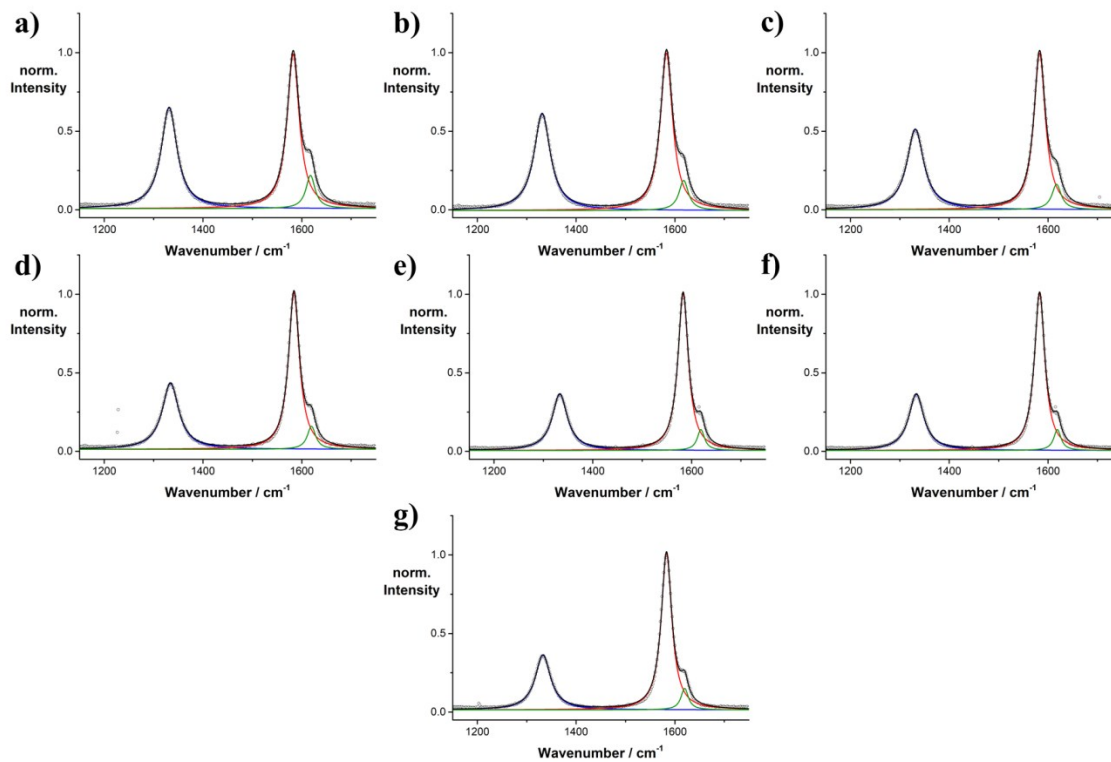


*Figure S6. Lorentz fitting of averaged Raman spectra of laser-reduced samples 1 – 7 (a – g).*

## Transmission electron microscopy and electron energy loss spectroscopy

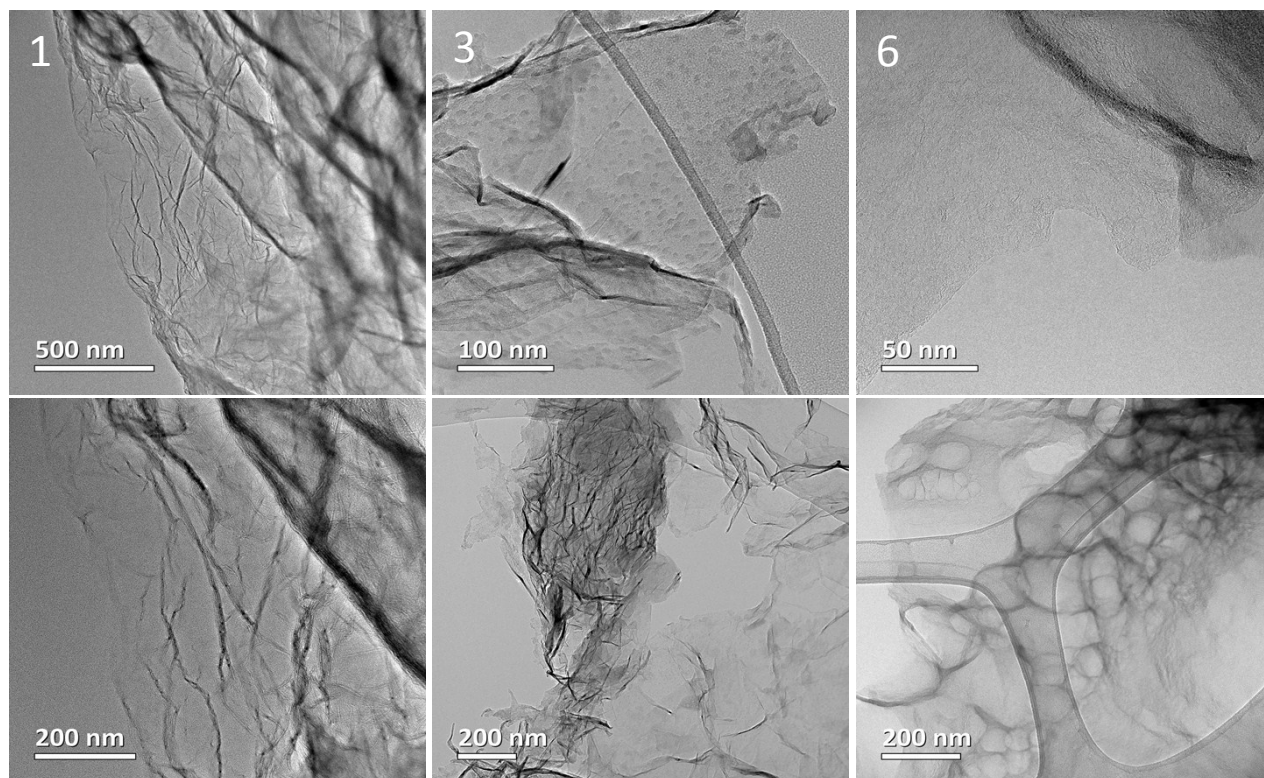


**Figure S7.** Representative TEM images of samples **1**, **3** and **6** obtained at an acceleration voltage of 200 kV.

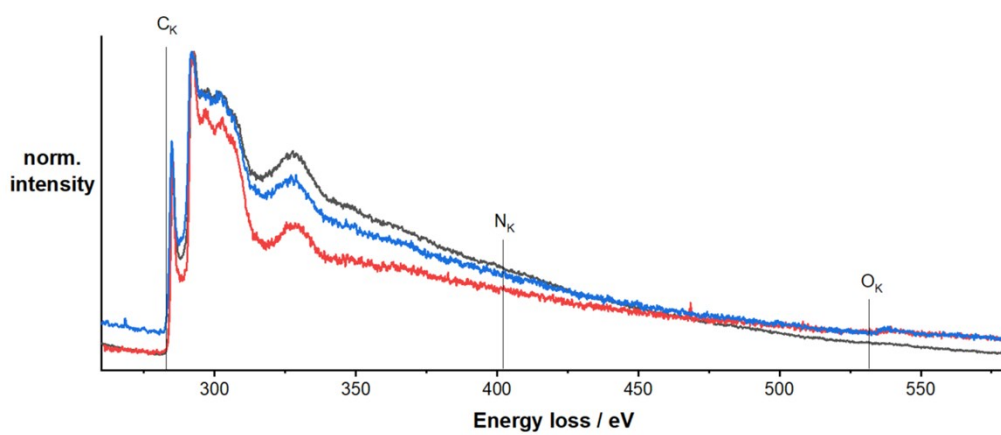


**Figure S8.** Electron energy loss spectra of samples **1** (black), **3** (red) and **6** (blue).

## Specific surface area measurements

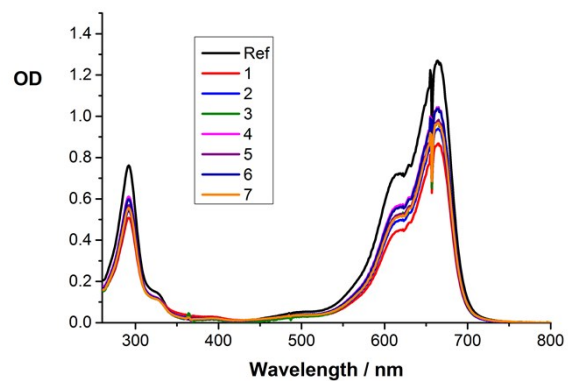


**Figure S9.** UV-vis absorption spectra of the methylene blue stock solution ( $c = 4.3 \times 10^{-5} M$ ) in black and the same solution after adsorbing  $\sim 0.1$  mg of samples **1** – **7**.

## Voltammetry



**Figure S10.** Photograph of the laser-reduced films on stainless-steel disks.

## Three-electrode measurements

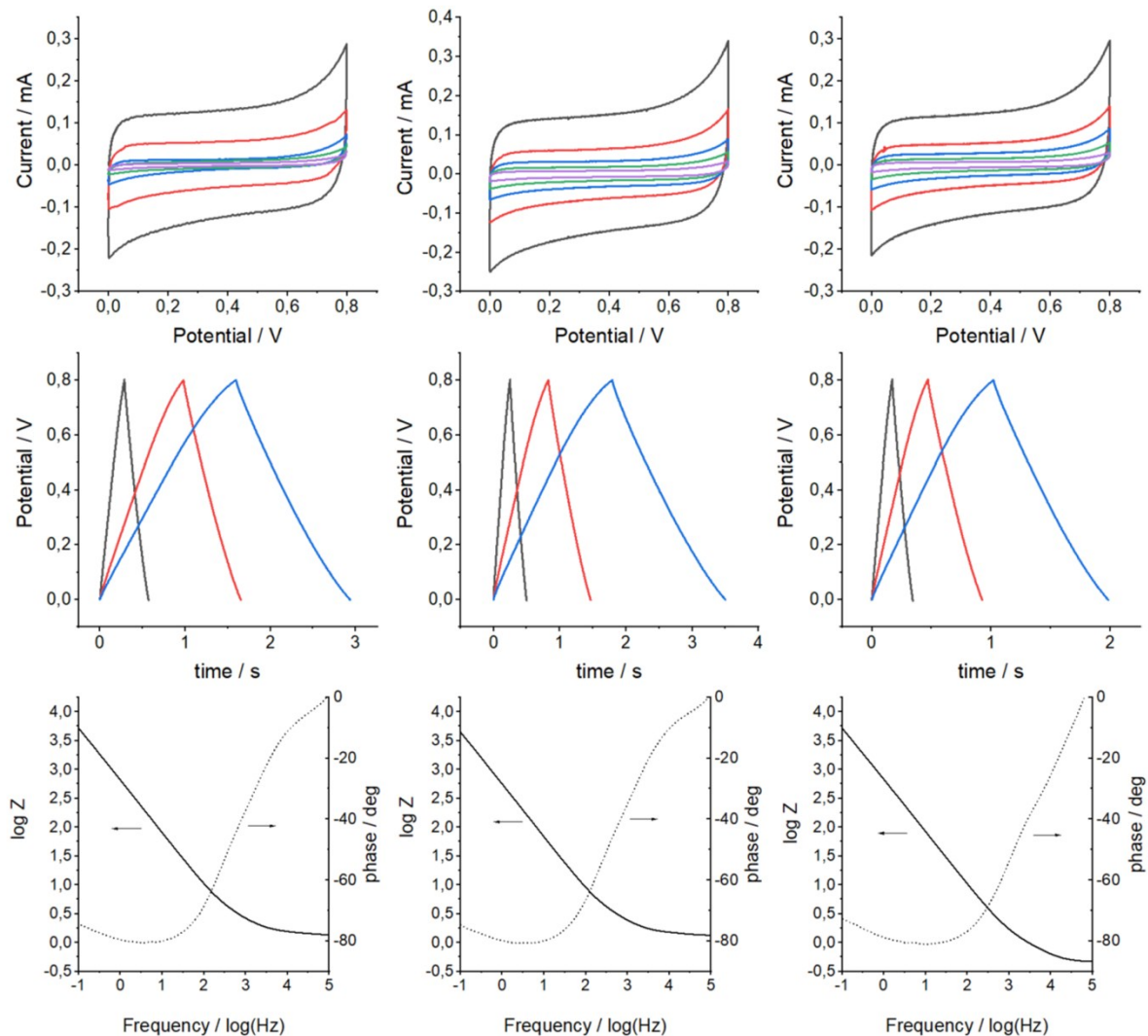


**Figure S11.** Electrochemical characterization electrodes fabricated from samples **1** (left column), **3** (center), and **6** (right) in 1.0 M  $\text{Na}_2\text{SO}_4$  using an Ag/AgCl reference electrode; a) Cyclic voltammograms in 1.0 M  $\text{Na}_2\text{SO}_4$  as electrolyte at different scan rates between 500 and 10  $\text{mV s}^{-1}$ ; b) Galvanostatic charge discharge curves obtained at different current densities of 7 (blue), 9 (red), and 10 ( $\text{Ag}^{-1}$ ) in 1.0 M  $\text{Na}_2\text{SO}_4$ ; c) Representative Bode impedance plots of the electrodes in 1.0 M  $\text{Na}_2\text{SO}_4$  as the electrolyte.

## Reference measurements in organic electrolyte

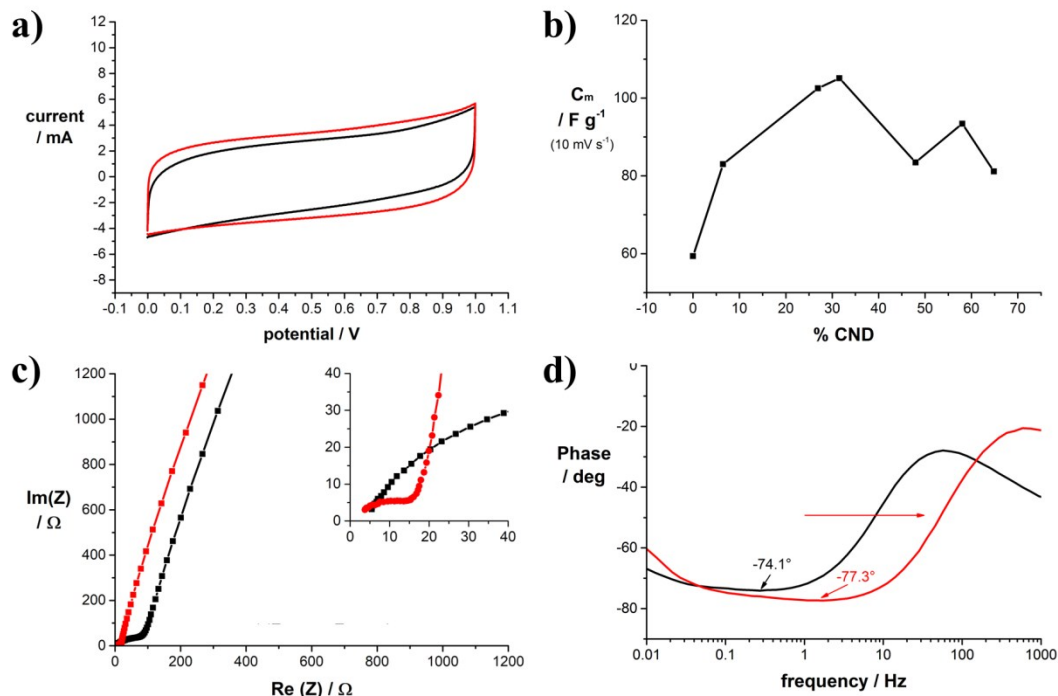


**Figure S12.** Electrochemical characterization of symmetric coin cell capacitors with different CND/GO mass ratios; a) Representative cyclic voltammograms of coin cell capacitors assembled with electrodes of sample 1 (black) and sample 5 (red) in 0.5 M TBAPF<sub>6</sub> in acetonitrile as electrolyte at a scan rate of 100 mV s<sup>-1</sup>; b) Specific gravimetric capacitance versus mass fraction of CNDs contained in the precursor solution determined by cyclic voltammetry at a scan rate of 10 mV s<sup>-1</sup>; c) Representative Nyquist impedance plots of coin cell capacitors assembled with electrodes of sample 1 (black) and sample 5 (red) in 0.5 M TBAPF<sub>6</sub> in acetonitrile as the electrolyte; d) Representative Phase-angle diagrams of coin cell capacitors assembled with electrodes of sample 1 (black) and sample 5 (red) in 0.5 M TBAPF<sub>6</sub> in acetonitrile as the electrolyte;

## Capacitance

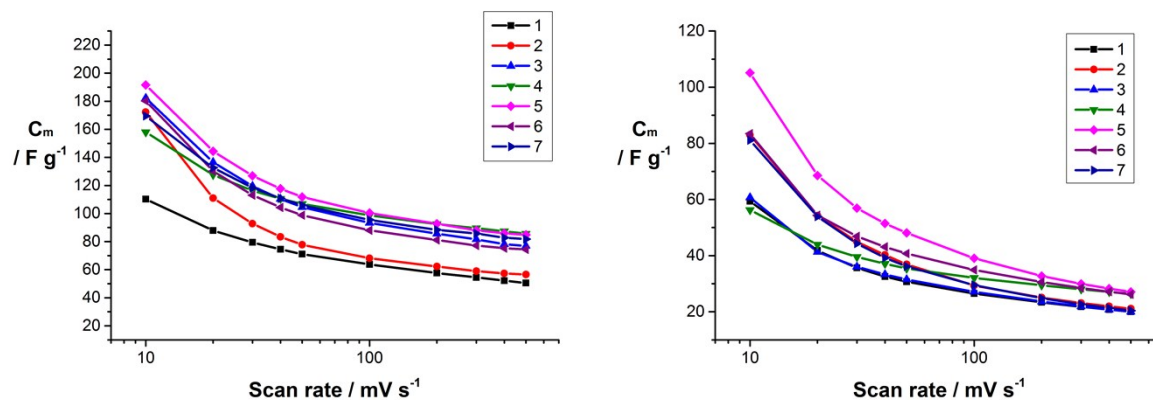


**Figure S13.** Specific gravimetric capacitances of samples 1 – 7 as a function of the scan rate in 6.0 M KOH (left) and in 0.5 M TBAPF<sub>6</sub> in acetonitrile as electrolyte (right).

## Galvanostatic charge-discharge measurements

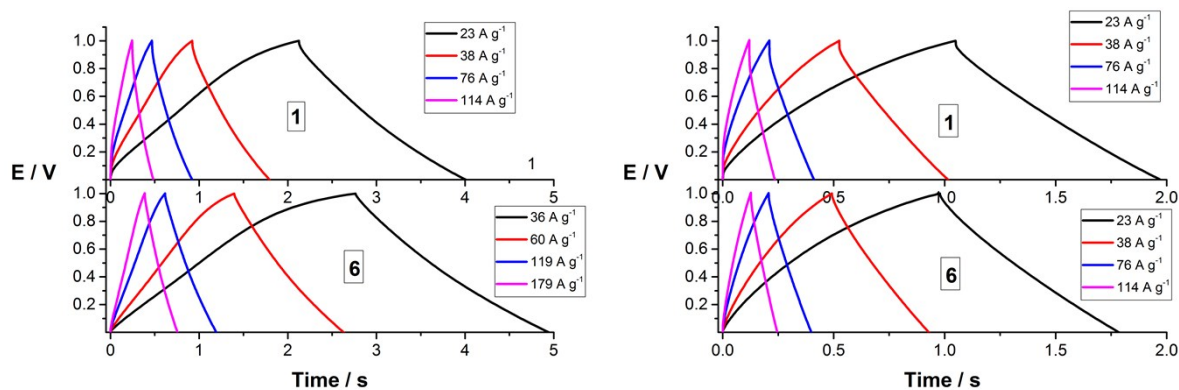


**Figure S14.** Galvanostatic charge discharge curves of samples **1** and **6** obtained at different current densities in 6.0 M KOH (left) and 0.5 M TBAPF<sub>6</sub> in acetonitrile (right).

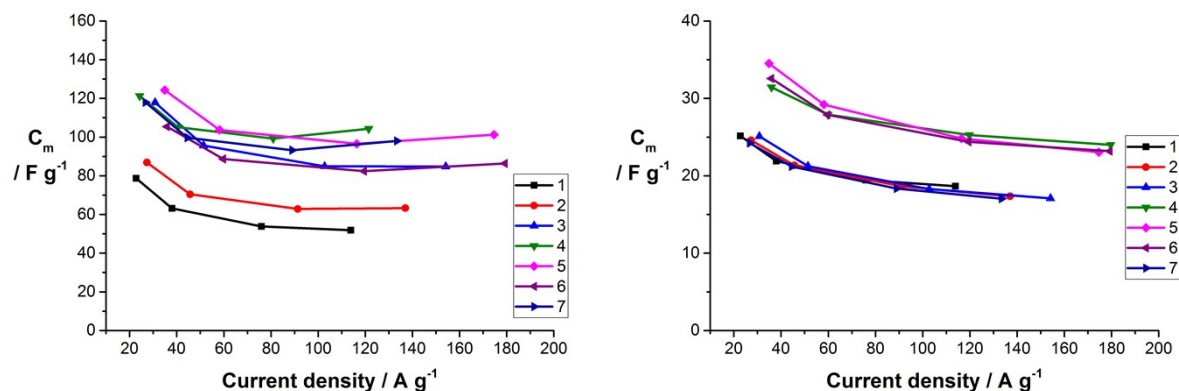


**Figure S15.** Specific gravimetric capacitances of samples **1** – **7** as a function of the current density in 6.0 M KOH (left) and in 0.5 M TBAPF<sub>6</sub> in acetonitrile as electrolyte (right).

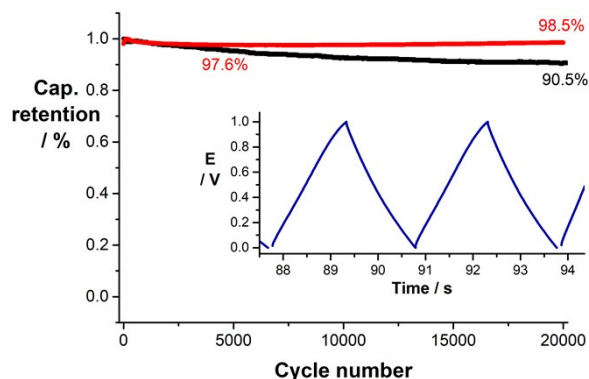


**Figure S16.** Capacitance retention of capacitor cells with sample **1** (black) and sample **6** (red) in 6.0 M KOH after 20,000 charge discharge cycles. Inset: Galvanostatic charge discharge curves of sample **6** obtained with a current density of 7.5 A g<sup>-1</sup>.

## Electrochemical impedance spectroscopy

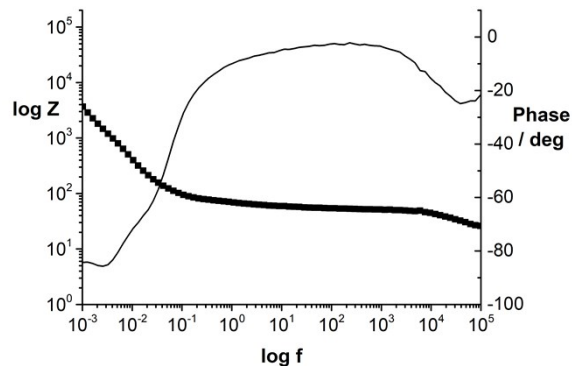


Figure S17. Representative Bode plot of a commercial activated carbon based EDLC.

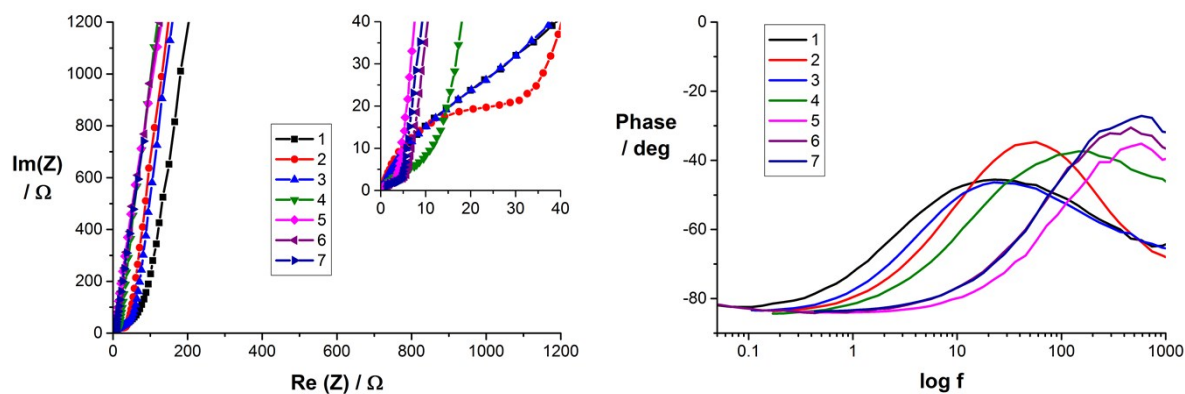


Figure S18. Left: Nyquist impedance plots of coin cell capacitors assembled with electrodes of samples 1 – 7 in 6.0 M KOH as electrolyte; Right: Phase angle plots of coin cell capacitors assembled with electrodes of samples 1 – 7 in 6.0 M KOH as the electrolyte.

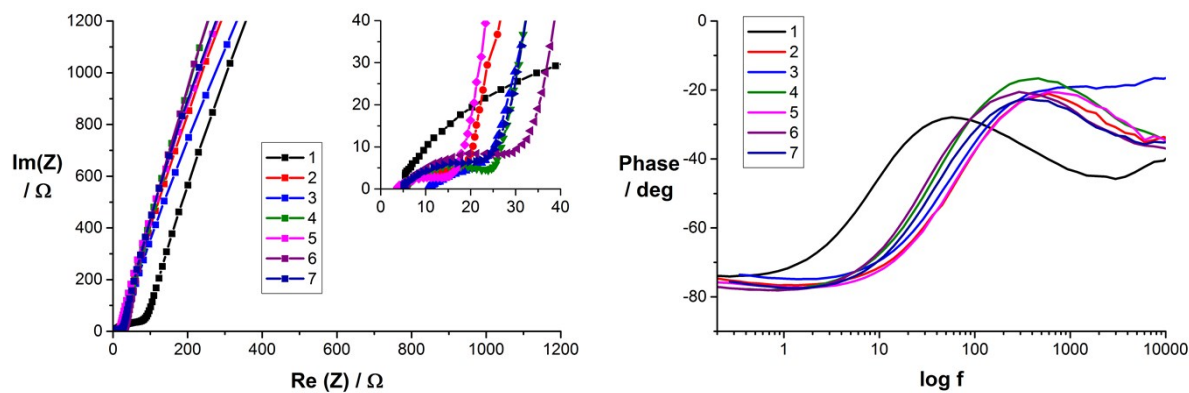


Figure S19. Left: Nyquist impedance plots of coin cell capacitors assembled with electrodes of samples 1 – 7 in 0.5 M TBAPF<sub>6</sub> in acetonitrile as the electrolyte; Right: Phase angle plots of coin cell capacitors assembled with electrodes of samples 1 – 7 with 0.5 M TBAPF<sub>6</sub> in acetonitrile as the electrolyte.